

A chaotic model for as a wake oscillator for flow induced vibrations of a rigid cylinder

Christophe Letellier

Rouen Normandie University — CORIA, Av. de l'Université, F-76800 Saint-Etienne du Rouvray, France

Luis A. Aguirre

†Laboratório de Modelagem, Análise e Controle de Sistemas Não Lineares

Departamento de Engenharia Eletrônica, Universidade Federal de Minas Gerais,

Av. Antônio Carlos 6627, 31270-901 Belo Horizonte, MG, Brazil

Guilherme Rosa Franzini & Celso Pupo Pesce

Laboratório de Mecânica Offshore, Escola Politécnica at University of São Paulo, SP, Brazil

(Dated: February 7, 2024, to submit.)

The flow-induced vibrations observed in a main cylinder are here investigated with the help of the dynamical system theory. The classical approach considers two bidirectionnally nonlinearly coupled oscillators for modeling this phenomenon: one oscillator is associated with vortex shedding and the second with cylinder displacement. The limitations in considering a van der Pol equation for the ~~vortex~~ oscillator and the advantages of a chaotic system instead of are here investigated.

I. INTRODUCTION

Flow of a fluid behind a body is a very complex phenomenon which can be characterized by means of some dimensionless numbers. For instance, when the Reynolds number Re is increased, the pattern of the flow behind a cylinder can be described as follows. For very low Re , the flow is laminar and independent of the time and, behind the cylinder, there is no separation of the flow. For $Re \approx 5$, three different domains within the flow are observed, that is, there are two vortices trapping some fluid particles in finite domain — the recirculation zone —, but the flow is still stable and laminar. For $Re_1 \approx 46$, the flow becomes time-dependent with the wake oscillating periodically [26]. There is a small transition for $Re_2 \approx 90$ for which vortex shedding dominates the vortex spacing and frequency [36]. For higher values of Re vortices or localized regions of high vorticity are shed alternately from either side of the cylinder and are convected downstream [14]. When $Re_3 \approx 189$, the flow loses its two-dimensional nature and three-dimensional patterns occurs [2]. In particular, the vortices can be dislocated and the velocity may clearly present aperiodic oscillations [40]. For these Reynolds numbers, new frequencies can be identified in the spectrum of the flow velocities, and ultimately, the flow becomes turbulent in the subcritical regime $10^3 < Re < 2 \cdot 10^5$ [18]. The details of the sequence of bifurcations between Re_1 and Re_3 are not yet well understood [2]. In this latter regime, the frequency of vortex shedding is nearly constant [6]. In the super-critical regime ($5 \cdot 10^5 < Re < 2 \cdot 10^6$), the wake has smaller amplitude than in the subcritical regime: it is even an open question whether there is yet vortex shedding within this range [18]. Moreover, the Strouhal frequency $St = \frac{f_D}{U}$ is almost constant [32].

The experimental observations do not provide a clear picture of the nature of the bifurcation between the first bifurcation leading to the periodic oscillations for $Re \approx$

50 and the vortex shedding. Batchelor comments this problem as follows [3]:

At a value of Re between 30 and 40, the steady flow appears to become unstable to small disturbances; [...] In the present case, the instability first affects the wake, at some distance downstream from the cylinder, and gives rise to a slow oscillation of the wake, approximately sinusoidal in both time and stream-wise distance, with an amplitude which increases with distance downstream. [...] As Re increases, beyond the critical value at which instability first appears, the oscillation in the wake moves closer to the cylinder and, when Re is near 60, begins to affect the two standing eddies immediately behind the cylinder.

When there is vortex shedding, the cylinder is affected by fluctuating lift force with the Strouhal frequency f_S . There is also a fluctuating drag force. One of the open problems is to describe the structural dynamics as a direct function of the cylinder and flow parameters. This is yet a topic of research due to the complexity of the interaction between the flow and the structure. This is even more complex when the cylinder has one degree of freedom, for instance, along the vertical axis. In this latter case, since the 1970s, the fluid behavior is described by heuristically proposed models, such as the van der Pol equation, that has been used for describing periodic vortex shedding [5, 11]. The validity of this model is controversial since it is justified only in the neighborhood of the first Hopf bifurcation where vortex shedding is periodic [1], that is, for $Re < Re_2$.

The present problem of flow-induced vibrations results from a mechanical problem coupled to a problem in fluid mechanics. Nevertheless, there is an actual component related to the nonlinear dynamical systems theory to interpret these interactions between a structure and a flow.

Indeed, the route to turbulence is already described with the help of this theory [2, 7]. This is the aim of this contribution. The subsequent part of this paper is organized as follows. In Section II, the classical model with a van der Pol equation is investigated with the help of the nonlinear dynamical systems theory. In Section III, an alternate three-dimensional chaotic system is proposed and some new features it induces are described. Section IV gives some conclusions.

II. THE COMMON WAKE OSCILLATOR

Our purpose is to investigate a phenomenological model for vortex-induced vibration of an elastically mounted cylinder in fluid flow. The degree of freedom is along the vertical axis. If we consider that the Reynolds number is still moderate ($Re \approx 100$), before the appearance of additional frequencies in the spectrum of flow velocities, it is commonly considered that the wake dynamics can be modeled with a van der Pol equation [11, 13]

$$\ddot{q} + \epsilon (q^2 - 1) \dot{q} + q = A \ddot{y}, \quad (1)$$

where q is the fluctuating lift coefficient on the structure. It is useful to note that measuring the velocity behind the cylinder at a point located with a height equal to the centre of the cylinder would provide a variable governed with the same underlying dynamics as vortex shedding. The van der Pol oscillator is known to produce nearly-linear oscillations (low ϵ -value) and relaxation oscillation ($\epsilon > 1$) [37] [Fig. 1].

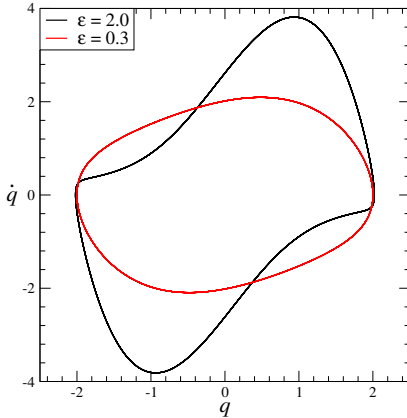


Figure 1: Limit cycle produced by the van der Pol oscillator (1) when $A = 0$ for two different values of ϵ .

Since it was proposed in an heuristic way, this model has no direct link with the Navier-Stokes equation [1] In spite of this, it is in agreement with the existence of a Hopf bifurcation at a Reynolds number $Re_H \approx 45$ at which oscillations of the wake occurs [5, 31]. The use of the van der Pol equation is justified only in the vicinity of the Hopf bifurcation, that is, where the be-

havior is strictly periodic, although such a phenomenological model is applied, with a relative success, for a range of Reynolds numbers far beyond the Hopf bifurcation [1]. This seems to be motivated by the fact that the Strouhal frequency does not strongly depend on the Reynolds number for $10^3 < Re < 10^4$. Nevertheless, this implicitly assumes that the behavior remains periodic, as shown in the super-critical regime, for instance [15, 32]. The parameter ϵ of the van der Pol equation and the coupling parameter A between the cylinder displacement and vortex shedding are tuning parameters, that is, they are tuned — in a heuristic way — to correspond to a given vortex shedding [30].

If this van der Pol equation can be considered as a model for fluctuating nature of the vortex street [29], it should be clear that it is valid as long as the vortex shedding remains periodic, at least when the dynamics underlying cylinder displacement is considered. Since the measured frequency is dependent on the fluid force on the cylinder, the wake oscillator is coupled to an equation for the adimensional displacement y of the cylinder with a diameter D [8]

$$\ddot{y} + 2\zeta \dot{y} + y = (\alpha q - \beta \dot{y}) \sqrt{1 + \delta \dot{y}^2}, \quad (2)$$

where

$$\begin{aligned} \alpha &= \frac{1}{2\pi^3} \frac{V_r^2}{m* + C_a^{\text{pot}}} \frac{\hat{C}_L^0}{\hat{q}} & \beta &= \frac{V_r}{m* + C_a^{\text{pot}}} \frac{C_{D,v}}{\pi^2} \\ \delta &= \left(\frac{2\pi}{V_r} \right)^2 & V_r &= \frac{V_\infty}{f_n D}. \end{aligned}$$

The displacement of the cylinder is normalized by the amplitude \hat{q}_y of the oscillations produced by the vortex shedding, that is, here, by the amplitude of the limit cycle produced by the van der Pol oscillator. \hat{C}_L^0 and $C_{D,v}$ are the amplitude of the lift coefficient and the mean drag coefficient in the flow around a fixed cylinder, respectively. ζ is a viscous damping coefficient. C_a^{pot} is the potential added mass coefficient for a cylinder immersed in infinite domain [38]. $m*$ is the mass ratio. Note that this oscillator is also equivariant under an inversion symmetry, that is, the dynamics is invariant under the coordinate change $(X, Y) \mapsto (-X, -Y)$.

Setting $X = y$, $Y = \dot{y}$, $Z = q$, and $W = \dot{q}$, the wake oscillator can be rewritten as a set of four ordinary differential equations in the form

$$\begin{cases} \dot{X} = Y \\ \dot{Y} = -X - 2\zeta Y + (\alpha Z - \beta Y) \sqrt{1 + \delta Y^2} \\ \dot{Z} = W \\ \dot{W} = -Z + \epsilon (1 - Z^2) W + A \dot{Y}. \end{cases} \quad (3)$$

This system has a jacobian matrix reading

$$\mathcal{J} = \begin{bmatrix} 0 & 1 & 0 & 0 \\ -1 & -2\zeta - \beta\sqrt{1+\delta Y^2} + \frac{(\alpha Z - \beta Y)\delta Y}{\sqrt{1+\delta Y^2}} & \alpha\sqrt{1+\delta Y^2} & 0 \\ 0 & 0 & 0 & 1 \\ -A & A \left(-2\zeta - \beta\sqrt{1+\delta Y^2} + \frac{(\alpha Z - \beta Y)\delta Y}{\sqrt{1+\delta Y^2}} \right) & -1 + A\alpha\sqrt{1+\delta Y^2} - 2\epsilon ZW & \epsilon(1-Z^2) \end{bmatrix} \quad (4)$$

which can be transformed into the symbolic Jacobian matrix

$$\tilde{\mathcal{J}} = \begin{bmatrix} 0 & 1 & 0 & 0 \\ 1 & \bar{1} & \bar{1} & 0 \\ 0 & 0 & 0 & 1 \\ 1 & \bar{1} & \bar{1} & \bar{1} \end{bmatrix} \quad (5)$$

where 1 stands for constant element J_{ij} , $\bar{1}$ for polynomial elements J_{ij} , and $\bar{\bar{1}}$ for rational elements J_{ij} [21]. From this jacobian matrix, the fluence graph is drawn as sketched in Fig. 2(a). An observability path is defined as a path through all the variables of a system with linear links [24]. The final end of the observability path is associated with the location of the sensor and its dual — in the Kalman [16] and Lin [27] sense —, that is, its initial end, is the variable the derivative of which receives the actuator. Only retaining linear edges, there are two distinct observability paths, one in each oscillator [Fig. 2(b)]. The final end of the observability path is associated with the location of the sensor and its dual — in the Kalman [16] and Lin [27] sense —, that is, its initial end, is the variable the derivative of which receives the actuator. Only retaining linear edges, there are two distinct observability paths, one in each oscillator [Fig. 2(b)]. In fact, for the cylinder oscillator, the observability path $X \rightarrow Y$ could be also retained from the graphical point of view, nevertheless, when it is better to avoid to measure a variable whose derivative is governed by nonlinear monomials, nonlinearities propagating quickly within the computation for observability. Consequently, two sensors must be placed, one at the displacement X of the cylinder and, one at the fluctuating lift Z .

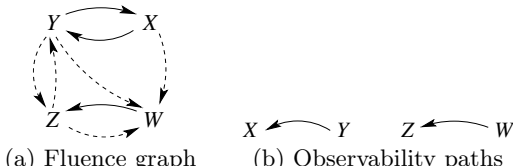


Figure 2: Fluence graph of the wake oscillator.

When the two variables X and Z are measured, the observability matrix

$$\tilde{\mathcal{O}}_{X^2Z^2} = \begin{bmatrix} 1 & 0 & 0 & 0 \\ 0 & 1 & 0 & 0 \\ 0 & 0 & 1 & 0 \\ 0 & 0 & 0 & 1 \end{bmatrix} \quad (6)$$

has a determinant equal to 1: measuring these two variables provides a global observability of the state space. This implies that besides the displacement of the cylinder, a variable providing informations related to the dynamics of the vortex shedding should be measured.

In experiments where there is cylinder displacement, the variable which is measured is X and more rarely a variable related to vortex shedding. It is therefore useful to state about the observability of the state space when only X is measured. In such a case, the determinant of the corresponding observability matrix is $\text{Det } \mathcal{O}_{X^4} = \alpha^2(1 + \delta Y^2)$. It never vanishes but it is a function of Y^2 , and the observability is not strictly global. This is confirmed with the symbolic observability matrix [21]

$$\tilde{\mathcal{O}}_{X^4} = \begin{bmatrix} 1 & 0 & 0 & 0 \\ 0 & 1 & 0 & 0 \\ 1 & \bar{1} & \bar{1} & 0 \\ \bar{1} & \bar{1} & \bar{1} & \bar{1} \end{bmatrix} \quad (7)$$

whose symbolic determinant is $\text{Det } \tilde{\mathcal{O}}_{X^4} = 1 \otimes 1 \otimes \bar{1} \otimes \bar{1}$. The symbolic observability coefficient [4, 25] is thus

$$\eta_{X^4} = \frac{2}{4} + \frac{2}{4^2} = 0.63 < 0.75, \quad (8)$$

meaning that, since the threshold of 0.75 is retained for a good observability of the state space [34], this variable offers a poor observability of the four-dimensional state space $\mathbb{R}^4(X, Y, Z, W)$. When only variable Z is measured, the observability matrix \mathcal{O}_{Z^4} is awfully complicated as well as its determinant: the symbolic approach is required to conclude. The symbolic observability matrix

$$\tilde{\mathcal{O}}_{Z^4} = \begin{bmatrix} 0 & 0 & 1 & 0 \\ 0 & 0 & 0 & 1 \\ 1 & \bar{1} & \bar{1} & \bar{1} \\ \bar{1} & \bar{1} & \bar{1} & \bar{1} \end{bmatrix} \quad (9)$$

has a symbolic determinant $\text{Det } \tilde{\mathcal{O}}_{Z^4} = 1 \otimes 1 \otimes (1 \otimes \bar{1} \oplus \bar{1} \otimes \bar{1})$. The corresponding symbolic observability coefficient is

$$\eta_{Z^4} = \frac{3}{6} + \frac{3}{6^2} = 0.58, \quad (10)$$

confirming that measuring variable Z provides a poorer observability of the state space than measuring variable X .

The wake oscillator (3) has a single singular point located at the origin of the state space. When evaluated at this point, the jacobian matrix (11) reduces to

$$\mathcal{J} = \begin{bmatrix} 0 & 1 & 0 & 0 \\ -1 & -2\zeta - \beta & \alpha & 0 \\ 0 & 0 & 0 & 1 \\ -A & A(-2\zeta - \beta) & -1 + A\alpha & \epsilon \end{bmatrix}. \quad (11)$$

With the parameter values reported in Table I, the corresponding eigenvalues are

$$\begin{cases} \lambda_1 = -0.554 \\ \lambda_2 = -1.806 \\ \lambda_{3,4} = 0.15 \pm 0.989i \end{cases} \quad (12)$$

The singular point is therefore a saddle-focus point. If the two oscillators are uncoupled ($A = 0$ and $\alpha = 0$), the eigenvalues can be expressed as a function of the parameters as follows.

$$\begin{cases} \lambda_{X,Y} = \frac{-(\beta+\zeta) \pm \sqrt{(\beta+2\zeta)^2 - 4}}{2} \\ \lambda_{Z,W} = \frac{\epsilon \pm \sqrt{\epsilon^2 - 4}}{2} \end{cases} \quad (13)$$

Replacing the parameters by their values as reported in Table I leads to the same numerical values as those reported in Eq. (12). This means that, for the retained parameter values, the dynamics of the two oscillators remains quite uncoupled. From the eigenvalues (13), let us determine the oscillating condition for each of the oscillators. From $\lambda_{X,Y}$, the oscillating condition is

$$|\beta + 2\zeta| < 2. \quad (14)$$

With the reported parameter values ($\beta \approx 0.36$), this suggests $|\zeta| < 0.82$ and the singular point is a stable focus point. From the eigenvalues $\lambda_{Z,W}$, the oscillating condition for the van der Pol oscillator is $|\epsilon| < 2$, leading to a singular point that is an unstable focus point.

Table I: Default parameter values for the wake oscillator (3). The last parameter, ζ , is very small, that is, fulfilling the oscillating condition and the corresponding monomial could even be removed from the equations. The retained value of V_r corresponds to $\text{Re} = 7800$.

$V_r = 6.39$	$D = 44.45 \text{ mm}$	$m* = 2.6$
$\hat{C}_L^0 = 2$	$C_{D,V} = 2$	$C_a^{\text{pot}} = 1$
$\epsilon = 0.3$	$\hat{q} = 2$	$A = 12$

From the state portrait plotted in Fig. 3(a), it can be seen that when $A = 12$, the coupling between the vortex shedding and the cylinder displacement is sufficiently strong to induce relaxation oscillation (compare the oscillations of the vortex shedding in Fig. 3(a) with the limit cycle produced by the isolated van der Pol oscillator (1) for $\epsilon = 2$ in Fig. 1). Note that the cylinder displacement  also associated with relaxation oscillations as revealed by the limit cycle which is very different from an ellipse. When the coupling from the cylinder displacement to the vortex shedding is decreased ($A = 0.1$), the “linear” limit cycle produced by the isolated van der Pol equation is recovered as plotted in Fig. 3(b).

To investigate the dependence of the amplitude of the limit cycle produced by these two coupled oscillators, we

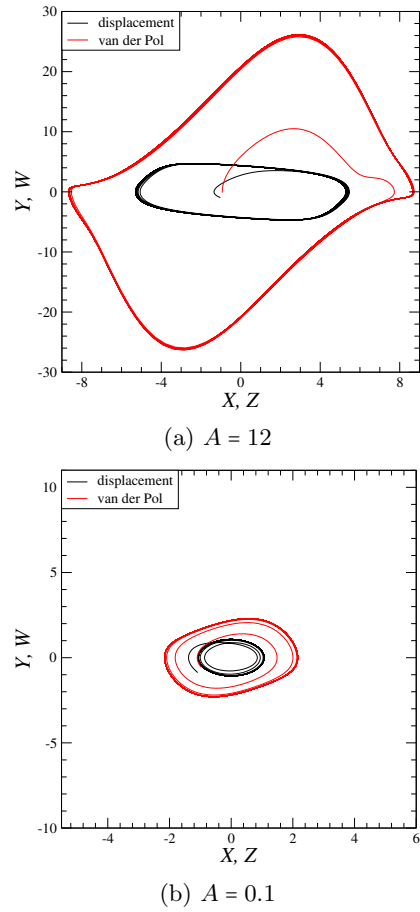


Figure 3: State portrait for the two coupled oscillators. $\zeta = 0.1$, $\alpha = 0.1829$, and other parameter values (if not specified) as reported in Table I.

computed a bifurcation diagram as a function of the A -value. The Poincaré section is associated with the maximum of the measured variable for each oscillator. In both cases, the amplitude increases with the A -value (Fig. 4). Since the van der Pol equation is also considered for large Reynolds number such as $10^3 < \text{Re} < 10^4$, that is, a range for which the flow is turbulent and some apparently “random” fluctuations appear in the flow, let us add noise ($\chi = 0 \pm 0.0029$) to the variable Z during the integration of the system. Increasing A leads to slightly larger fluctuations in the cylinder displacement (compare the fluctuations in the amplitude X_n with those in the amplitude Z_n plotted in Fig. 4).

The evolution of the amplitudes as a function of A plotted in Fig. 4 suggests that a rather simple relationship between them could be obtained. We therefore plotted Z_n as a function of X_n : the plot is adequately fitted by a quadratic function as shown in Fig. 5: as long as the vortex shedding remains periodic, a condition for which, the van der Pol equation is valid, there is a simple relationship between it and the cylinder displacement.

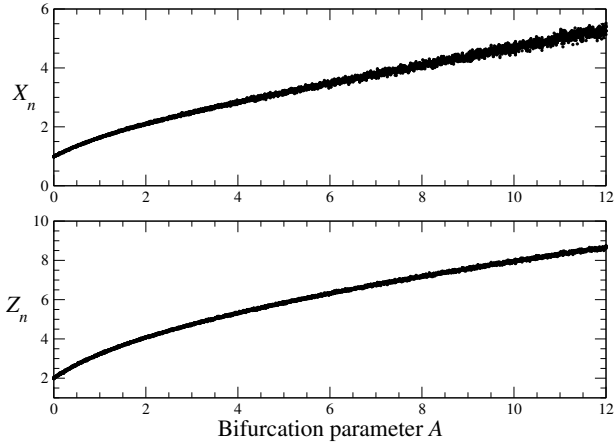


Figure 4: Bifurcation diagram of the wake oscillator with a noisy Z -variable (noise of $\chi = 0 \pm 0.0029$ added to the variable Z during the integration). $\zeta = 0.1$, and other parameter values as reported in Table I.

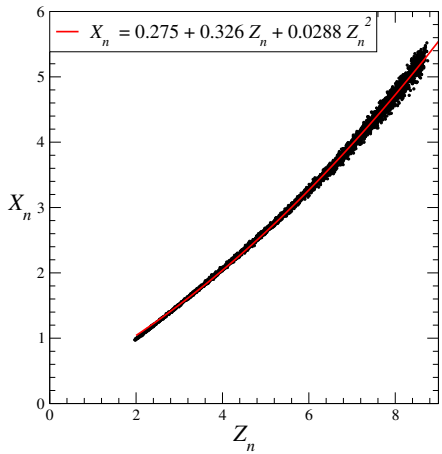


Figure 5: Amplitude X_n of the cylinder displacement as a function of the amplitude Z_n of the vortex shedding when the A values are varied over the range [2, 12]. $\zeta = 0.1$, and other parameter values as reported in Table I.

III. ANOTHER MODELLING CHOICE

Since, for Reynolds number roughly greater than 200, the vortex shedding is no longer periodic [15, 39], it would be natural to replace the van der Pol equation by another oscillator that can produce more complex dynamics. Since in vortex shedding, there is a symmetry along the flow, with one bottom vortex between two consecutive top vortices, and *vice versa*, it is natural to introduce an oscillator which presents such a symmetry. Let us therefore consider the case where the van der Pol system is replaced with the Burke and Shaw system [35]

$$\begin{cases} \dot{x} = -x + y \\ \dot{y} = -\frac{y}{\sigma} - xz \\ \dot{z} = \frac{\xi}{\sigma} + xy \end{cases} \quad (15)$$

where $\sigma = 10$ and $\xi = 4.272$ [22]. This system presents an order-2 rotation symmetry around the z_{BS} -axis. Such a symmetry allows to consider the alternation of vortex shedding with respect to the cylinder. To the best of our knowledge, the route to turbulence in the flow behind the cylinder is still not clarified [2]. Note that a period-doubling bifurcation was observed for $Re \approx 300$ [17]. Chaotic behavior was observed in a similar model but with two piecewise linear switches [12]. In another configuration, chaotic dynamics were observed in vortex-induced vibrations of flexible risers [28]. These three examples provide an additional motivation for the choice of the chaotic Burke-Shaw system in place of the van der Pol equation.

For the parameter values indicated above, the behavior is chaotic: an example of the x -time series is plotted in Fig. 6. The governing equations used as a heuristic model for aperiodic wake are now associated with a three-dimensional state space. This chaotic model will therefore allow to “simulate” aperiodic vortex shedding.

In the context of experiments in which there is no direct measurements for the vortex shedding, it is important to couple the vortex oscillator with the cylinder oscillator through the variable of the former offering the best observability of its state space, that is, of its dynamics [19]: this would help to an easier characterization of the dynamics underlying the fluid and, consequently, of the cylinder oscillator. From the fluence graph of the Burke-Shaw system, we may obtain the observability path $z \rightarrow y \rightarrow x$, leading to measure the variable x [24]. Note that, here, the connexion between z and y is in fact nonlinear: it is therefore not possible to get global observability from the measurement of a single variable since the nonlinear link between y and z necessarily induces a singular observability manifold [9, 20]. Indeed, when the variable x of the Burke-Shaw system is measured, the observability matrix

$$\mathcal{O}_{x^3} = \begin{bmatrix} 1 & 0 & 0 \\ -1 & -1 & 0 \\ 1+z & 1+\frac{1}{\sigma} & x \end{bmatrix} \quad (16)$$

has for determinant $\text{Det}\mathcal{O}_{x^3} = -x$; its symbolic counterpart is $\text{Det}\tilde{\mathcal{O}}_{x^3} = 1 \otimes 1 \otimes \bar{1}$, leading to a symbolic observability coefficient $\eta_{x^3} = 0.78 > 0.75$: the variable x thus provides a good observability of the state space associated with the Burke-Shaw system. According the observability path (when the nonlinear connexion $z \rightarrow y$ is not removed), the dual of the variable x is the derivative \dot{z} (duality principle introduced by Kalman [16] and Lin [27]). Thus, when the actuating signal is applied to derivative \dot{z} of the Burke-Shaw system, the determinant

of the controllability matrix

$$\mathcal{C}_{\dot{z}} = \begin{bmatrix} 0 & 0 & x \\ 0 & x & \left(\frac{1}{\sigma} - 1\right)x - y \\ 1 & 0 & -x^2 \end{bmatrix} \quad (17)$$

is $\text{Det}\mathcal{C}_{\dot{z}} = -x^2$. The determinant of the symbolic controllability matrix $\tilde{\mathcal{C}}_{\dot{z}}$ is equal to $1 \otimes 1 \otimes \bar{1}$, leading to a symbolic controllability coefficient $\eta_{\dot{z}} = 0.78 > 0.75$: according to it, the controllability of the Burke-Shaw system through \dot{z} is good. It is interesting to note that $\text{Det}\mathcal{C}_{\dot{y}} = -2x$ but that $\text{Det}\tilde{\mathcal{C}}_{\dot{y}} = 1 \otimes (1 \otimes \bar{1} \oplus \bar{1} \otimes 1)$, leads to $\eta_{\dot{y}} = 0.68$, that is, the controllability through \dot{y} is poor. Applying the control (or the coupling) on the derivative \dot{z} of the Burke-Shaw system is therefore optimal from the controllability point of view. The actuator is thus placed at \dot{z} , meaning that the coupling of the oscillator for the cylinder displacement is coupled to the Burke-Shaw system through \dot{z} .

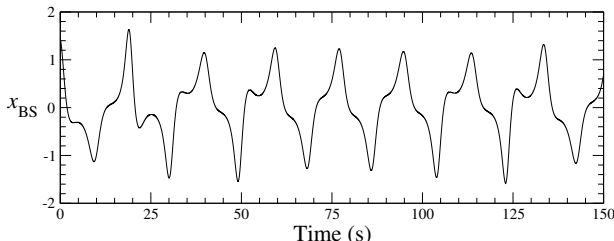


Figure 6: x -time series produced by the Burke-Shaw system (15). Parameter values: $\sigma = 10$ and $\xi = 4.272$.

When a bifurcation diagram is computed as a function of ξ (Fig. 7), it presents successive period-doubling cascades leading to chaotic attractors. The first, the third, and the fifth ones start after a pitchfork bifurcation breaking the symmetry of the limit cycle that occurred with a saddle-node bifurcation. Then, a classical period-doubling cascade takes place, leading to an asymmetric chaotic attractor. Due to the rotation symmetry, replacing the initial conditions according to $(x_0, y_0, z_0) \mapsto (-x_0, -y_0, z_0)$ leads to the co-existing companion attractor. An attractor merging crisis between these two co-existing chaotic attractors arises. The resulting attractor is characterized by a sudden increase in its size. The single symmetric resulting attractor is hereafter developed up to a boundary crisis followed by a new saddle-node bifurcation. The second and the fourth period-doubling cascades emerge after a saddle-node bifurcation giving birth to an axi-symmetric limite cycle and ends as the three others. This bifurcation diagram will serve as a reference for discussing the diagram obtained with the five-dimensional wake oscillator (18).

When the vortex shedding is modeled by the Burke-

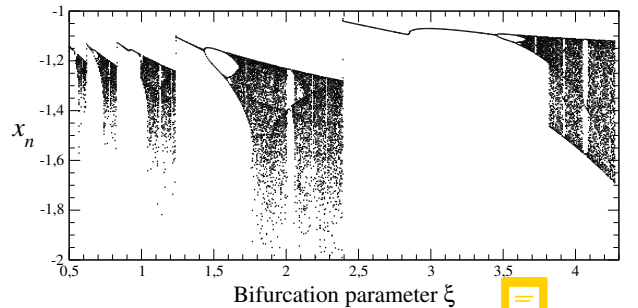


Figure 7: Bifurcation diagram as a function of the parameter ξ of the Burke-Shaw system (15). Other parameter value: $\sigma = 10$.

Shaw system, the wake oscillator reads as

$$\begin{cases} \dot{X} = Y \\ \dot{Y} = -X - 2\zeta Y + (\alpha x_{\text{BS}} - \beta Y) \sqrt{1 + \delta Y^2} \\ \dot{x}_{\text{BS}} = -x_{\text{BS}} + y_{\text{BS}} \\ \dot{y}_{\text{BS}} = -\frac{y_{\text{BS}}}{\sigma} - x_{\text{BS}} z_{\text{BS}} \\ \dot{z}_{\text{BS}} = \frac{\xi}{\sigma} + x_{\text{BS}} y_{\text{BS}} + A \dot{Y} \end{cases} \quad (18)$$

and is five-dimensional. Note that the observability of the state space is now associated with $\text{Det}\mathcal{O}_{X^5} = \alpha^3(1 + \delta Y^2)^{3/2}x$, and a corresponding symbolic observability coefficient $\eta_{X^5} = 0.52$: the observability of the dynamics underlying flow-induced vibration is therefore poor when the sole variable measured is the cylinder displacement. In other words, the more complex the vortex shedding, the less observable the state space from a single measured variable.

When there is no feedback from the cylinder displacement to the vortex shedding ($A = 0$), the Burke-Shaw system (15) produces a chaotic attractor [Fig. 8(a)] characterized by a four-branch first-return map [Fig. 8(b)]. Such a map is obtained from the two-component Poincaré section [10, 23]

$$\mathcal{P}_{\text{BS}} \equiv \{(x_n, y_n) \in \mathbb{R}^2 \mid \dot{x}_{\text{BS}} = 0, \ddot{x}_{\text{BS}} \leq 0, x_{\text{BS}} \gtrless \pm 0.75\} \quad (19)$$

where the x_{BS} is normalized on each component within the unit interval and oriented from the centre to the periphery of the attractor [33]: one component is thus within $[-1, 0[$ and the other within $]0, 1]$. The obtained first-return map exhibits the fact that the Burke-Shaw attractor has two foldings occurring in series, with an odd global torsion between each [22]. The fact that the displacement dynamics is fed by the vortex shedding, the state portrait [Fig. 8(c)] associated with the linear oscillator (2) for the cylinder displacement is also with an order-2 symmetry: as a result the Poincaré section has also two components and should present similar features as in Fig. 8(b).

When the trajectory is projected in the sub-space $\mathbb{R}^2(X, Y)$, it describes an attractor which looks quite

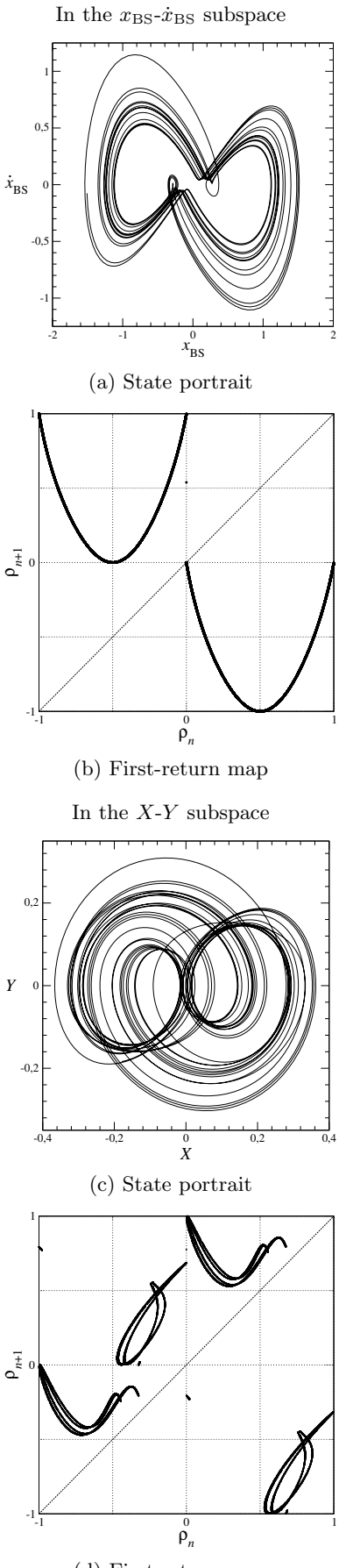


Figure 8: First-return map for the two coupled oscillators. $\zeta = 0.1$, $\alpha = 0.1829$, $A = 0$, and other parameter values as reported in Table I.

different from the Burke-Shaw attractor [compare Fig. 8(a) with Fig. 8(c)] but still with an order-2 symmetry as mentioned above. To avoid numerical problems, the two-component Poincaré section is now defined as

$$\mathcal{P}_{\text{XY}} \equiv \{(X_n, Y_n) \in \mathbb{R}^2 \mid Y = 0, \dot{Y} \leq 0, X \geq \pm 0.36\}. \quad (20)$$

The first-return map to this Poincaré section is plotted in Fig. 8(d). We recover the two smooth unimodal maps (with a minimum) but located at different places with respect to the first bisecting line: this is due to the possibility to reinject the trajectory within the same “wing”, a feature which cannot be observed in the Burke-Shaw attractor. This would mean that, although the vortices occurs alternately top and bottom with respect to the cylinder, the cylinder displacement does not necessary obey this pattern: the cylinder would be able to oscillate twice around the same position. In the first-return map, this is characterized by the “foliated loops” (roughly for $-0.5 < \rho_n < 0$ and for $0.5 < \rho_n < 1.0$). The interactions between the flow and the cylinder are in such a way that the resulting dynamics underlying cylinder displacement do not follow linearly the dynamics underlying vortex shedding.

Let us start to investigate how the Burke-Shaw system affects the dynamics of the cylinder displacement in setting $A = 0$ [Fig. 9(c)]. Comparing this diagram with the bifurcation diagram obtained with the Burke-Shaw system [Fig. 7], it is possible to assess how the cylinder oscillator is affected by the vortex oscillator. We recover the five period-doubling cascade, but with different number of branches. For instance, when $2.5 < \xi < 3.5$, there is a single branch in the bifurcation diagram of the isolated Burke-Shaw system and three in the cylinder oscillator. This comes from the fact that, in the cylinder oscillator, there is a possibility to reinject the trajectory in the same wing, a feature that is not possible in the Burke-Shaw system. Moreover, the trajectory visits twice the Poincaré section in the cylinder oscillator when it visits a single time the Poincaré section \mathcal{P}_{BS} . Apart from that, the cylinder dynamics is conjugated to the vortex dynamics. When $A \neq 0$, the two systems are coupled in a bidirectional way. This induces a development of the dynamics which corresponds to a shift in the parameter space toward the small ξ -values. The sequence of bifurcations is also affected or even removed. For instance, the sequence observed for $1.77 \leq \xi \leq 2.39$ and $A = 0$ [Fig. 9(a)] is removed when $A = 0.77$ [Fig. 9(b)]. The two coupled oscillators should be considered as a global system, each being affected by the other. The flexibility of chaotic behavior reveals that the interplay between these two oscillators is complex and cannot be investigated as a simple superimposition of two distinguishable (separable) dynamics.

When $\xi = 4.271$ [Fig. 9(c)], increasing the coupling A develops the dynamics underlying vortex shedding into a more complex attractor (it could be shown that the first-return map has more than four-branches). If some noise is added on the derivative \dot{z}_{BS} , increasing the A -

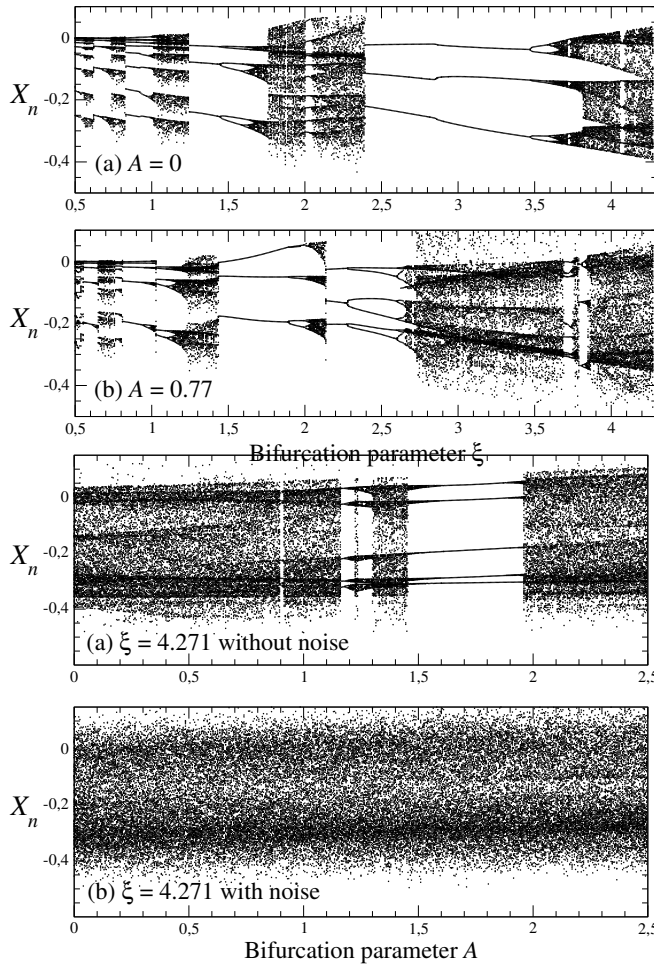


Figure 9: Bifurcation diagram as a function of A for $\xi = 4.271$ — for noise free vortex shedding (a) and with noise (b) — as a function of ξ for two values of A (b) and (c)]. The Poincaré section used for computing these diagrams is one of the two components of \mathcal{P}_{BS} . Other parameter values as reported in Table I.

value does not exhibit any clear bifurcation [Fig. 9(d)]: all the dynamics looks similar since they are blurred by the noise contamination. Since this noise could be considered as, for instance, the “random” fluctuations due to turbulence, when the interactions between the two oscillators are drown in a sea of noise, it is no longer possible to distinguish different regime and the A -value does no longer have any meaning.

As a last computation, we computed a bifurcation diagram as a function of the reduced velocity V_r , with a van der Pol oscillator [Fig. 10(a)] and with a Burke-Shaw oscillator [Fig. 10(b)] as a vortex oscillator, respectively. In the former case, increasing the velocity V_r leads to an increase in the amplitude of oscillations which remain strictly periodic. Contrary to this, a Burke-Shaw vortex oscillator leads to a more developed chaotic regime, that is, the underlying dynamics becomes more complex, although the main frequency is nearly constant, and with

larger fluctuations [Fig. 10(b)]. The bidirectional coupling — equivalent to a closed feedback loop — between the vortex and the cylinder oscillators combined with the chaotic nature of the vortex oscillators are the two relevant ingredients for such results.

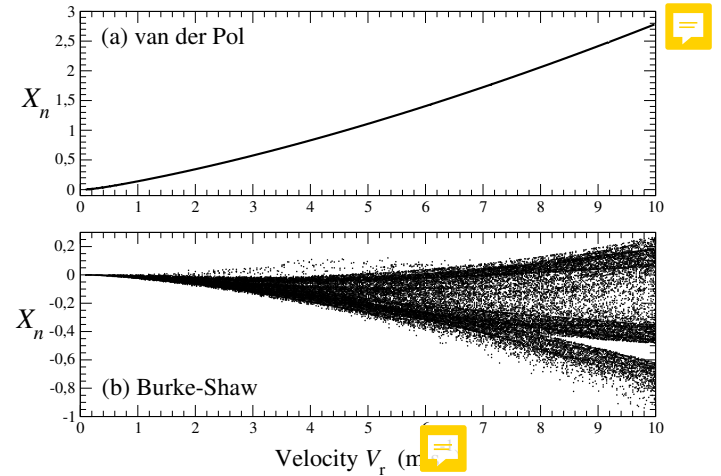


Figure 10: Bifurcation diagram as a function of V_r with $A = 0.77$ for the van der Pol system (a) and the Burke-Shaw system(b). Other parameter values as reported in Table I.

IV. CONCLUSION

The complex dynamics governing flow-induced vibrations are here investigated in the case where a cylinder is free to move along a vertical axis. Its displacements result from nonlinear couplings between a vortex oscillator and a cylinder oscillator. Although only justified in the neighborhood of an initial Hopf bifurcation leading to periodic vortex shedding, a van der Pol oscillator is commonly considered for modeling this phenomenon, even when large Reynolds number, necessarily associated with more complex dynamics. We here showed that such two-dimensional oscillator provides a limited number of types of dynamics whose simplicity — limit cycle being noisy or not — does not match with some experimental evidences. We therefore replaced this too simple model with a chaotic system, here the Burke-Shaw system, which presents the advantage to produce, when isolated, an alternation between two wings, each of them being phenomenologically associated with top and bottom vortices. Its chaotic nature and the associated sensitivity to initial conditions exhibits that richer dynamics can be produced by the coupled vortex and cylinder oscillators. In particular, it is shown that, a purely deterministic system can predict an increase in the amplitude of cylinder displacements when the reduced velocity of the flow is increased, a result which cannot be obtained with a van der Pol model. Such a result exhibits the stability of the nonlinear dynamics theory to open new doors in the difficult problem of modeling flow-induced vibrations.

Acknowledgements

This work has been supported by FAPES.

- [1] J. A. P. ARANHA : Weak three dimensionality of a flow around a slender cylinder: the Ginzburg-Landau equation. *Journal of Brazilian Society of Mechanical Sciences and Engineering*, 26(4), 2004.
- [2] D. BARKLEY et R. D. HENDERSON : Three-dimensional Floquet stability analysis of the wake of a circular cylinder. *Journal of Fluid Mechanics*, 322:215–241, 1996.
- [3] G. K. BATCHELOR : *An introduction to fluid dynamics*. Cambridge University Press, 2000.
- [4] E. BIANCO-MARTINEZ, M. S. BAPTISTA et C. LETELLIER : Symbolic computations of nonlinear observability. *Physical Review E*, 91(6):062912, 2015.
- [5] R. E. D. BISHOP, A. Y. HASSAN et O. A. SAUNDERS : The lift and drag forces on a circular cylinder oscillating in a flowing fluid. *Proceedings of the Royal Society of London A*, 277(1368):51–75, 1964.
- [6] M. S. BLOOR : The transition to turbulence in the wake of a circular cylinder. *Journal of Fluid Mechanics*, 19(2):290–304, 1964.
- [7] B. ECKHARDT et H. FAISST : Dynamical systems and the transition to turbulence. In T. MULLIN et R. KERSWELL, éds : *IUTAM Symposium on Laminar-Turbulent Transition and Finite Amplitude Solutions*, p. 35–50, Dordrecht, 2005. Springer Netherlands.
- [8] M. L. FACCHINETTI, E. DE LANGRE et F. BIOLLEY : Coupling of structure and wake oscillators in vortex-induced vibrations. *Journal of Fluids and Structures*, 19(2):123–140, 2004.
- [9] M. FRUNZETE, J.-P. BARBOT et C. LETELLIER : Influence of the singular manifold of nonobservable states in reconstructing chaotic attractors. *Physical Review E*, 86(2):026205, 2012.
- [10] R. GILMORE et C. LETELLIER : *The symmetry of chaos*. Oxford University Press, New York, 2007.
- [11] R. T. HARTLEN et I. G. CURRIE : Lift-oscillator model of vortex-induced vibration. *Journal of the Engineering Mechanics Division*, 96(5):577–591, 1970.
- [12] B. HUYNH, T. TJAHHOWIDODO, Z.-W. ZHONG, Y. WANG et N. SRIKANTH : Design and experiment of controlled bistable vortex induced vibration energy harvesting systems operating in chaotic regions. *Mechanical Systems and Signal Processing*, 98:1097–1115, 2018.
- [13] W. D. IWAN et R. D. BLEVINS : A model for vortex induced oscillation of structures. *Journal of Applied Mechanics*, 41(3):581–586, 1974.
- [14] C. P. JACKSON : A finite-element study of the onset of vortex shedding in flow past variously shaped bodies. *Journal of Fluid Mechanics*, 182:23–45, 1987.
- [15] H. JIANG et L. CHENG : Transition to chaos in the cylinder wake through the mode C flow. *Physics of Fluids*, 32(1):014103, 2020.
- [16] R. KALMAN : On the general theory of control systems. *IFAC Proceedings Volumes*, 1(1):491–502, 1960. 1st International IFAC Congress on Automatic and Remote Control, Moscow, USSR, 1960.
- [17] G. E. KARNIADAKIS et G. S. TRIANTAFYLLOU : Three-dimensional dynamics and transition to turbulence in the wake of bluff objects. *Journal of Fluid Mechanics*, 238:1–30, 1992.
- [18] O. LEHMKUHL, I. RODRGUEZ, R. BORRELL, J. CHIVA et A. OLIVA : Unsteady forces on a circular cylinder at critical Reynolds numbers. *Physics of Fluids*, 26(12):125110, 2014.
- [19] C. LETELLIER, L. AGUIRRE et J. MAQUET : How the choice of the observable may influence the analysis of nonlinear dynamical systems. *Communications in Nonlinear Science and Numerical Simulation*, 11(5):555–576, 2006.
- [20] C. LETELLIER et L. A. AGUIRRE : Graphical interpretation of observability in terms of feedback circuits. *Physical Review E*, 72(5):056202, 2005.
- [21] C. LETELLIER et L. A. AGUIRRE : Symbolic observability coefficients for univariate and multivariate analysis. *Physical Review E*, 79(6):066210, 2009.
- [22] C. LETELLIER, P. DUTERTRE, J. REIZNER et G. GOUESBET : Evolution of multimodal map induced by an equivariant vector field. *Journal of Physics A*, 29:5359–5373, 1996.
- [23] C. LETELLIER et R. GILMORE : Covering dynamical systems: Two-fold covers. *Physical Review E*, 63(1):016206, 2001.
- [24] C. LETELLIER, S. MANGIAROTTI, L. MINATI, M. FRASCA et J.-P. BARBOT : Optimal placement of sensor and actuator for controlling low-dimensional chaotic systems based on global modeling. *Chaos*, 33(1):013140, 2023.
- [25] C. LETELLIER, I. SENDIÑA-NADAL, E. BIANCO-MARTINEZ et M. S. BAPTISTA : A symbolic network-based nonlinear theory for dynamical systems observability. *Scientific Reports*, 8:3785, 2018.
- [26] J. H. LIENHARD : Analysis of lift, drag, and vortex frequency data for rigid circular cylinders. Rap. tech. 300, Bulletin of the Washington State University, Washington State University, 1966.
- [27] C.-T. LIN : Structural controllability. *IEEE Transactions on Automatic Control*, 19(3):201–208, 1974.
- [28] Y. MODARRES-SADEGHI, F. CHASPARIS, M. S. TRIANTAFYLLOU, M. TOGNARELLI et P. BEYNET : Chaotic response is a generic feature of vortex-induced vibrations of flexible risers. *Journal of Sound and Vibration*, 330(11):2565–2579, 2011.
- [29] A. H. NAYFEH : *Introduction to perturbation techniques*. Wiley, New York, 1993.
- [30] R. H. M. OGINK et A. V. METRIKINE : A wake oscillator with frequency dependent coupling for the modeling of vortex-induced vibration. *Journal of Sound and Vibration*, 329(26):5452–5473, 2010.
- [31] M. PROVANSAL, C. MATHIS et L. BOYER : Bénard-von Kármán instability: transient and forced regimes. *Journal of Fluid Mechanics*, 182:1–22, 1987.
- [32] I. RODRGUEZ, O. LEHMKUHL, J. CHIVA, R. BORRELL et A. OLIVA : On the flow past a circular cylinder from critical to super-critical Reynolds numbers: Wake topology

- and vortex shedding. *International Journal of Heat and Fluid Flow*, 55:91–103, 2015.
- [33] M. ROSALIE et C. LETELLIER : Systematic template extraction from chaotic attractors: i. Genus-one attractors with an inversion symmetry. *Journal of Physics A*, 46(37):375101, 2013.
- [34] I. SENDIÑA-NADAL, S. BOCCALETTI et C. LETELLIER : Observability coefficients for predicting the class of synchronizability from the algebraic structure of the local oscillators. *Physical Review E*, 94(4):042205, 2016.
- [35] R. SHAW : Strange attractor, chaotic behavior and information flow. *Zeitschrift für Naturforschung A*, 36:80–112, 1981.
- [36] D. J. TRITTON : Experiments on the flow past a circular cylinder at low Reynolds numbers. *Journal of Fluid Mechanics*, 6(4):547–567, 1959.
- [37] B. van der POL : On “relaxation-oscillations”. *Philosophical Magazine*, 2(11):978–992, 1926.
- [38] K. VIKESTAD, J. K. VANDIVER et C. M. LARSEN : Added mass and oscillation frequency for a circular cylinder subjected to vortex-induced vibrations and external disturbance. *Journal of Fluids and Structures*, 14(7):1071–1088, 2000.
- [39] R. F. WILLIAMS : The structure of Lorenz attractors. *Publications Mathématiques de l'I.H.E.S.*, 50:73–99, 1979.
- [40] C. H. K. WILLIAMSON : Three-dimensional wake transition. In S. GAVRILAKIS, L. MACHIELS et P. A. MONKEWITZ, éds : *Advances in Turbulence VI*, p. 399–402, Dordrecht, 1996. Springer Netherlands.